Research Article Vol. 58, No. 36 / 20 December 2019 / Applied Optics 9757

applied optics

Hybrid two-level MPPM–*M*DPSK modulation for high-speed optical communication networks

Haitham S. Khallaf,[1,2,*,†] Ahmed E. Morra,[3,4,†] Abdulaziz E. Elfiqi,[4,†] Hossam M. H. Shalaby,[5,6] and Steve Hranilovic[3]

[1]Nuclear Research Center, Egyptian Atomic Energy Authority (EAEA), Inshas 13759, Egypt
[2]Graduate School of Information Science and Electrical Engineering, Kyushu University, Fukuoka, Japan
[3]Department of Electrical and Computer Engineering, McMaster University, Ontario L8S 4K1, Canada
[4]Electronics and Electrical Communications Engineering Department, Faculty of Electronic Engineering, Menoufia University, Menouf 32952, Egypt
[5]Electrical Engineering Department, Faculty of Engineering, Alexandria University, Alexandria 21544, Egypt
[6]Department of Electronics and Communications Engineering, Egypt-Japan University of Science and Technology E-JUST, Alexandria 21934, Egypt
*Corresponding author: eng.h.khallaf@gmail.com

Received 15 August 2019; revised 29 October 2019; accepted 30 October 2019; posted 31 October 2019 (Doc. ID 375073); published 11 December 2019

A hybrid optical modulation approach is described, which layers a continuous wave *M*–ary differential phase-shift keying (*M*DPSK) and a two-level ($2L$) multipulse pulse-position modulation (MPPM) intensity-modulated signal for improved spectral efficiency. These $2L$ techniques are a generalization of earlier hybrid MPPM–*M*DPSK techniques and have the added advantage of reducing transmitter and detector complexities over previous hybrid modulation approaches. The spectral and power efficiencies for the proposed $2L$-MPPM–*M*DPSK modulation techniques are formulated and shown to have the highest spectral efficiency in comparison to other hybrid techniques with lower implementation complexity. The performance of the proposed $2L$ hybrid techniques is quantified over free-space optical (FSO) networks as well as fiber networks and verified using Monte Carlo simulation. For FSO channels, the proposed $2L$-MPPM–*M*DPSK technique outperforms the traditional MPPM–*M*DPSK scheme by approximately 2 dB at a bit-error rate (BER) of 10^{-4} and a spectral efficiency of 2.5 bit/s/Hz. Similarly, in optical fiber, the proposed scheme relaxes the impact of nonlinearity in comparison to traditional MPPM–*M*DPSK. Specifically, at a BER$= 10^{-3}$, the $2L$-MPPM–*M*DPSK technique outreaches the MPPM–*M*DPSK by 2000 km at a spectral efficiency of 2.5 bit/s/Hz and an average transmit power of -3 dBm.

https://doi.org/10.1364/AO.58.009757

1. INTRODUCTION

Hybrid optical modulation approaches, which combine spectrally efficient techniques, e.g., phase-based modulation techniques, with power-efficient intensity methods, e.g., position-based modulation, have been shown to simultaneously achieve high spectral and power efficiencies [1–23]. These hybrid optical modulation techniques have been investigated in numerous scenarios using both coherent [1–5] and direct detection [6–9] receivers. A comparison among existing hybrid modulation work is summarized in Table 1. Although coherent approaches offer greater sensitivity, this comes at the expense of great complexity due to the required local oscillator and carrier recovery subcircuits at the receiver. Intensity approaches {e.g., intensity-modulated (IM)-quadrature amplitude modulation (QAM) (IM-QAM) [8,9] and hybrid asymmetrically clipped optical orthogonal frequency-division multiplexing (ACO-OFDM)–on–off keying (OOK) modulation technique [10]} modulate the envelope of the carrier and have lower sensitivity while requiring complex analog-to-digital converters for electrical detection. In [22], a combination of electrical code division-multiplexing access (ECDMA) and OFDM was proposed for low-cost, low-complexity, and high-speed passive optical networks (PONs) with the first demonstration of an analogue OFDM ECDMA. While in [23], to handle the practical issue of timing jitter, hybrid multi-band (HMB) carrierless amplitude and phase (CAP)/QAM transmitter/receiver systems have been proposed. A more attractive approach [6,7] is to use differential phase-shift keying (DPSK), which allows for the detection of the differential phase in the optical domain, along with a multipulse pulse-position modulation (MPPM) detector. This approach has the advantage of high-power efficiency and

Table 1. Survey of Hybrid Modulation Techniques Considering Receiver Complexity

Technique	Detection Type	All-Optical Receiver?
[1–5]	Coherent (PSK+PPM/MPPM)	Yes
[8,9]	Direct (IM-QAM+MPPM)	No
[10]	Direct (ACO-OFDM+OOK)	No
[6,7]	Direct (DPSK+MPPM)	Yes
[11–18]	Direct (DPSK+ASK)	Yes
This work	Direct (DPSK + 2LMMPM)	Yes

having an all-optical direct-detection receiver; however, a highly complex ultrafast optical variable delay line is needed due to the discrete nature of the DPSK over the MPPM frame.

Another variant of DPSK-based modulation techniques, termed amplitude-shift keying-MDPSK (ASK–MDPSK), has been proposed to encode multiple bits per symbol. [11–18]. This scheme is based on ASK and thus is less power efficient than PPM-based approaches. Additionally, the rate of ASK–MDPSK cannot be easily adapted, while MPPM approaches allow greater rate flexibility, which is especially attractive in time-varying free-space optical (FSO) channels. In addition to atmospheric turbulence, time-varying optical communication channels can arise in many scenarios including coronal turbulence (deep space FSO channels) [24,25] and oceanic turbulence (underwater wireless optical channels) [26,27].

In this paper, we introduce an adaptive hybrid two-level (2L)-MPPM and DPSK optical modulation format, which improves the spectral efficiencies of earlier work [1–9] while reducing transmitter and receiver complexities [28]. While the spectral efficiencies of the proposed technique and ASK–MDPSK are nearly the same, 2L-MPPM–MDPSK is more power efficient than ASK–MDPSK and can work as an adaptive modulation technique in time-varying channels, such as FSO channels. The key idea is that DPSK-modulated signals are superimposed on binary-level MPPM with amplitude signaling levels set to A_h and A_l, which are not necessarily zero (as in Fig. 1, where $\mathbb{R}e\{\cdot\}$ denotes the real operator). We term these approaches as 2L-MPPM–MDPSK to emphasize that the binary intensity levels are specified arbitrarily in the design. Notice that, unlike [6,7], if $A_l > 0$, the DPSK symbols are sent continuously in time. This greatly improves the spectral efficiency over [6,7], since more degrees of freedom are present in the output signal for modulation. Additionally, the continuous transmission of DPSK symbols for $A_l > 0$ allows for the removal of the complex variable delay line in [6,7], which greatly simplifies the receiver architecture. In addition, position-based and phase-based modulation techniques are transmitted independently in contrast to the previous hybrid modulation techniques [1–9], which results in simplified transmitter and receiver processing units.

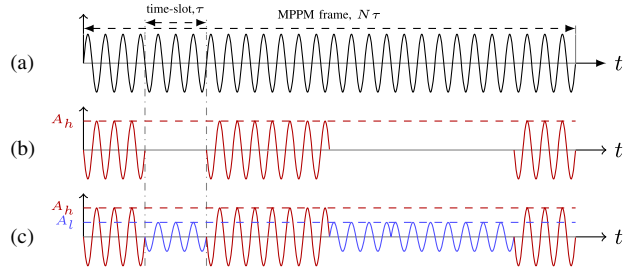

Fig. 1. Time-frame waveforms of $\mathbb{R}e\{\cdot\}$ part of optical signals for (a) continuous-wave laser, (b) MPPM–MDPSK [6,7], and (c) 2L-MPPM–MDPSK signals, with $N = 8$ and $w = 4$.

The spectral and power efficiencies of the 2L-MPPM–DPSK technique are presented and compared to earlier approaches. In order to illustrate the utility of this approach, the performance of the hybrid 2L-MPPM–DPSK modulation approaches is quantified and shown to be a good choice for realistic FSO and fiber networks. Closed-form expressions are given for the bit-error rate (BER) and outage probability of the 2L-MPPM–MDPSK scheme on FSO channels in the presence of scintillation. Using the Gaussian noise (GN) model for nonlinearity [29], both the BER and maximum reach of fiber systems are presented for our 2L-MPPM–DPSK modulation formats. In addition, analytical expressions for the power efficiency, outage probability, and BER are derived for earlier hybrid ASK–MDPSK schemes [11–18] under both FSO and fiber channels as a special case of the proposed 2L-MPPM–DPSK modulation scheme. It is shown that the proposed hybrid 2L-MPPM–DPSK modulation formats offer both practical improvements in the reliability of FSO links and increased reach of fiber links, while reducing transmitter and receiver complexities.

The balance of the paper is organized as follows. In Section 2, 2L-MPPM–MDPSK is defined and transmitter and receiver structures are outlined. In Section 3, the spectral and power efficiencies are discussed and evaluated. In Section 4, BER and outage probability for the 2L-MPPM–MDPSK system over exponentiated Weibull (EW) turbulence FSO fading channels are derived and discussed. Performance analysis under fiber nonlinearities is explored and investigated in Section 5. Numerical results for both FSO and fiber channels are given in Section 6. Finally, conclusions are drawn in Section 7.

2. DEFINITION OF HYBRID 2L-MPPM–MDPSK

Figure 2 presents a block diagram of both the transmitter and receiver of the proposed 2L-MPPM–MDPSK schemes.

A. Transmitter

At the transmitter, a carrier is intensity modulated based on the 2L-MPPM symbols. As mentioned in Section 1, the 2L-MPPM symbol consists of N time slots with $N - w$ of them having low signal level, A_l, and w with high signal-level, A_h, where $P_l = A_l^2$ and $P_h = A_h^2$ are the average transmitted optical power in low-level and high-level time slots, respectively $(0 < P_l < P_h)$. Define

$$\delta = \frac{P_l}{P_h} \tag{1}$$

as the ratio of low-to-high signal-level intensities—alternatively, the inverse of the *transmitter extinction ratio*. The transmitter signal-processing unit (T-SPU) sends $\lfloor \log_2 \binom{N}{w} \rfloor$ bits for each 2L-MPPM symbol. Thus, in the kth time slot, the 2L-MPPM optical signal can be represented as

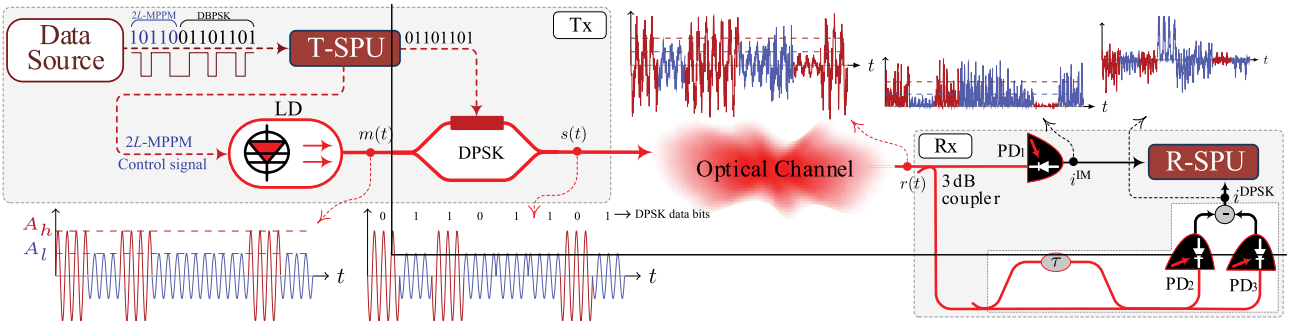

Fig. 2. Example of block diagram of proposed hybrid $2L$-MPPM–MDPSK modulation technique for $(N, w, M, \delta) = (8, 3, 2, 0.25)$. Tx, transmitter; Rx, receiver; LD, laser diode; PD, photodiode; T-SPU, transmitter signal-processing unit; R-SPU, receiver signal-processing unit. The time-frame waveforms are illustrated along different stages of the proposed system setup, where $\mathbb{R}\mathrm{e}\{m(t)\}$, $\mathbb{R}\mathrm{e}\{s(t)\}$, and $\mathbb{R}\mathrm{e}\{r(t)\}$ are plotted.

$$m_k(t) = a_k \exp(j\omega_c t), \tag{2}$$

where ω_c is the optical carrier frequency in rad/s, and the root mean square (RMS) of $m_k(t)$, $a_k \in \{A_l = \sqrt{P_l}, A_h = \sqrt{P_h}\}$, is selected according to $2L$-MPPM, as shown in Fig. 2, where $\mathbb{R}\mathrm{e}\{m(t)\}$ is plotted.

The IM carrier is then input into an MDPSK modulator that sends $\log_2 M$ bits per time slot by varying the differential phase of the carrier, as shown in Fig. 2, where M is the cardinality of the MDPSK modulation technique. Thus, the transmitted $2L$-MPPM–MDPSK optical signal in the kth time slot is

$$s_k(t) = a_k \exp(j(\omega_c t + \phi_k)), \tag{3}$$

where ϕ_k is the phase of the transmitted signal. In MDPSK, data are conveyed in the differences

$$\Delta\phi_k = \phi_k - \phi_{k-1} = (2i-1)\pi/M,$$

where $i \in \{1, 2, \ldots, M\}$.

Thus, for $2L$-MPPM–MDPSK, a data frame of length of $\lfloor \log_2 \binom{N}{w} \rfloor + N \log_2 M$ bits is fed to the T-SPU and transmitted in N consecutive time slots, compared with $\lfloor \log_2 \binom{N}{w} \rfloor + w \log_2 M$ bits for MPPM–MDPSK. The T-SPU manipulates these bits to control the operation of both the laser driving current (i.e., $2L$-MPPM signal) and the MDPSK modulator as discussed earlier.

B. Receiver

The received optical signal from FSO or optical fiber channels can be written, respectively, as

$$r_k(t) = \begin{cases} \sqrt{h} a_k \exp(j(\omega_c t + \phi_k)); & \text{for FSO,} \\ \left[a_k \exp(j\phi_k) + n_{tk}\right] \exp(j\omega_c t); & \text{for fiber,} \end{cases} \tag{4}$$

where h is the FSO channel gain, and $n_{tk} = \mathbb{R}\mathrm{e}\{n_{tk}\} + j\mathbb{I}\mathrm{m}\{n_{tk}\}$ is the lowpass representation of optical fiber channel noise described in Section 5. Given that the coherence time of atmospheric fading is many orders of magnitude larger than the symbol interval, we adopt a non-ergodic model for the channel-fading state and represent it as independent of time and EW distributed [30].

The received optical signal is spilt by a 3 dB coupler into two branches: one for IM and the other for MDPSK demodulation. In the case of IM MPPM, the photodiode (PD) converts the optical intensity variation into an electrical signal with electric current of

$$i_k^{\mathrm{IM}} = \begin{cases} \mathcal{R}\left|\frac{r_k(t)}{\sqrt{2}}\right|^2 + n_D; & \text{for FSO,} \\ \mathcal{R}\left|\frac{r_k(t)}{\sqrt{2}}\right|^2; & \text{for fiber} \end{cases},$$

$$= \begin{cases} \frac{\mathcal{R}}{2} h a_k^2 + n_D; & \text{for FSO,} \\ \frac{\mathcal{R}}{2}[a_k^2 + \mathbb{R}\mathrm{e}\{n_{tk}\}^2 + \mathbb{I}\mathrm{m}\{n_{tk}\}^2 + 2a_k & \text{for fiber,} \\ \times(\mathbb{R}\mathrm{e}\{n_{tk}\}\cos\phi_k + \mathbb{I}\mathrm{m}\{n_{tk}\}\sin\phi_k)], \end{cases} \tag{5}$$

where $\mathcal{R}$ is the detector responsivity, and n_D is the receiver thermal noise with variance σ_n^2 assuming a thermal-noise-limited scenario for the FSO channel case. Notice that in the case of optical fiber, it is assumed that receiver noises (shot and thermal noises) are negligible compared to optical noise sources, as described in Section 5.A. This current value is fed to the receiver signal-processing unit (R-SPU) as seen in Fig. 2. For MPPM, the R-SPU detects the received data by collecting N consecutive chip intervals and independently detecting the positions of the w high-signal-level time slots that contain the highest power.

On the MDPSK arm, (considering $M = 2$ as an example), traditional direct detection for the MDPSK signal is performed by employing an optical delay interferometer. The input optical signals of PD_2 and PD_3 for the Mach–Zehnder interferometer (MZI) are denoted $r_{2k}^{\mathrm{DPSK}}(t)$ and $r_{3k}^{\mathrm{DPSK}}(t)$, respectively, and can be written as

$$r_{2k}^{\mathrm{DPSK}}(t) = \frac{1}{2\sqrt{2}}(r_k(t) + r_k(t-\tau)), \tag{6a}$$

$$r_{3k}^{\mathrm{DPSK}}(t) = \frac{1}{2\sqrt{2}}(r_k(t) - r_k(t-\tau)), \tag{6b}$$

where $\tau = T/N$ is the time-slot duration, and T is the frame-time duration. The electric MDPSK current can be written as

$$i_k^{\mathrm{DPSK}} = \begin{cases} \mathcal{R}\left(|r_{2k}^{\mathrm{DPSK}}(t)|^2 - |r_{3k}^{\mathrm{DPSK}}(t)|^2\right) + n_D; & \text{for FSO,} \\ \mathcal{R}\left(|r_{2k}^{\mathrm{DPSK}}(t)|^2 - |r_{3k}^{\mathrm{DPSK}}(t)|^2\right); & \text{for fiber.} \end{cases} \tag{7}$$

In the R-SPU, the received data words are reconstructed independently from both the $2L$-MPPM and MDPSK decoded

Table 2. Spectral and Power Efficiencies for Different IM- and *M*DPSK-Based Modulation Techniques

Modulation Scheme	Spectral Efficiency [bit/s/Hz]	Power Efficiency
*M*DPSK	$\log_2 M$	$\log_2 M \sin^2(\frac{\pi}{M})$
MPPM	$\frac{\lfloor \log_2 \binom{N}{w} \rfloor}{N}$	$\frac{\lfloor \log_2 \binom{N}{w} \rfloor}{2w}$
MPPM–*M*DPSK [6,7]	$\frac{\lfloor \log_2 \binom{N}{w} \rfloor + w \log_2 M}{N}$	$\frac{\lfloor \log_2 \binom{N}{w} \rfloor + w \log_2 M}{w} \min\left\{\frac{1}{2}, \sin^2(\frac{\pi}{M})\right\}$
2*L*-MPPM–*M*DPSK	$\frac{\lfloor \log_2 \binom{N}{w} \rfloor + N \log_2 M}{N}$	$\frac{\lfloor \log_2 \binom{N}{w} \rfloor + N \log_2 M}{w+(N-w)\delta^2} \min\left\{\frac{(1-\delta)^2}{2}, \delta^2 \sin^2(\frac{\pi}{M})\right\}$
ASK–*M*DPSK [11–18]	$1 + \log_2 M$	$\frac{1+\log_2 M}{1+\delta^2} \min\left\{\frac{(1-\delta)^2}{2}, 2\delta^2 \sin^2(\frac{\pi}{M})\right\}$

data bits. This is a key point in simplifying the transmitter and receiver for the 2*L*-MPPM–*M*DPSK scheme, since variable delay lines are no longer required for DPSK detection as in [6,7] with simplified T-SPU and R-SPU in contrast to the previous hybrid modulation techniques [1–9]. Notice that for $M > 2$, the receiver in Fig. 2 requires that the *M*DPSK arm have two optical delay interferometers with phase difference of $\pi/2$ to be able to differentiate between inphase and quadrature components [31].

3. SPECTRAL AND POWER EFFICIENCIES

A. Spectral Efficiency

The spectral efficiency η_s is defined as [32]

$$\eta_s = \frac{R_b}{W} \quad \text{bit/s/Hz}, \tag{8}$$

where R_b is the transmission data rate in bits per second, and W is the system bandwidth. The spectral and power efficiencies of different IM- and *M*DPSK-based modulation techniques are summarized in Table 2. It can be observed that 2*L*-MPPM–*M*DPSK and ASK–*M*DPSK techniques have the highest spectral efficiencies in comparison with other hybrid modulation techniques. Indeed, this increase in the spectral efficiency comes at the expense of losing some power efficiency for $\delta > 0$.

B. Power Efficiency

The power efficiency γ is defined as [32]

$$\gamma = \frac{d_{\min}^2}{4\mathcal{E}_b}, \tag{9}$$

where $d_{\min}$ is the minimum Euclidean distance between two symbols in the constellation, $\mathcal{S}$, and $\mathcal{E}_b$ is the average energy per bit. For the case of 2*L*-MPPM–*M*DPSK, $\mathcal{E}_b$ and $d_{\min}$ are

$$\begin{aligned}\mathcal{E}_b &= E\left\{\int_0^T |x(t)|^2 \mathrm{d}t\right\} \cdot \frac{1}{\lfloor \log_2 \binom{N}{w} \rfloor + N \log_2 M} \\ &= \frac{w + (N-w)\delta^2}{\lfloor \log_2 \binom{N}{w} \rfloor + N \log_2 M} (\mathcal{R} P_b)^2 \tau,\end{aligned} \tag{10}$$

for any symbol $x(t) \in \mathcal{S}$, and

$$\begin{aligned}d_{\min}^2 &= \min_{\substack{x(t), z(t) \in \mathcal{S} \\ x(t) \neq z(t)}} \left\{\int_0^T |x(t) - z(t)|^2 \mathrm{d}t\right\} \\ &= (\mathcal{R} P_b)^2 \tau \min\left\{2(1-\delta)^2, 4\delta^2 \sin^2\left(\frac{\pi}{M}\right)\right\}.\end{aligned} \tag{11}$$

Accordingly, the power efficiency for the 2*L*-MPPM–*M*DPSK modulation scheme is

$$\gamma = \frac{\lfloor \log_2 \binom{N}{w} \rfloor + N \log_2 M}{w + (N-w)\delta^2} \min\left\{\frac{(1-\delta)^2}{2}, \delta^2 \sin^2\left(\frac{\pi}{M}\right)\right\}. \tag{12}$$

Similarly, for the ASK–*M*DPSK modulation technique [11–18], the power efficiency expression can be written as

$$\gamma = \frac{1 + \log_2 M}{1 + \delta^2} \min\left\{\frac{(1-\delta)^2}{2}, 2\delta^2 \sin^2\left(\frac{\pi}{M}\right)\right\}. \tag{13}$$

Figure 3 plots the spectral efficiencies of hybrid IM- and *M*DPSK-based modulation techniques versus the reciprocal of the power efficiency ($1/\gamma$), i.e., the *receiver sensitivity*, at different cardinality levels of *M*DPSK modulation technique $M \in \{2, 4, 8, 16\}$ for $w/N \in [0, 1]$ and $N = 20$. It can be seen from the figure that the 2*L*-MPPM–*M*DPSK technique has the highest power efficiency in the high-spectral-efficiency region ($\eta_s > 2.25$ bit/s/Hz). Notice that the maximum spectral efficiency for the 2*L*-MPPM techniques at any cardinality of the *M*DPSK is achieved when $w/N = 0.5$. Additionally, the value of δ must be selected for all 2*L* techniques to balance the power efficiency between 2*L*-MPPM and *M*DPSK modulations. Section 6 presents the method by which δ can be selected for FSO and fiber channels. The particular values of δ selected for all 2*L* techniques in Fig. 3 was found by a search to optimize γ. In the case of 2*L*-MPPM–*M*DPSK, the optimum δ is taken as the one that maximizes power efficiency at $w/N = 0.5$. Notice that as the DPSK cardinality increases, the value of δ must increase to compensate for the effect of increasing M on power efficiency Eq. (12).

In addition to the benefits listed above, 2*L*-MPPM–*M*DPSK techniques can be considered as adaptive modulation techniques, which helps in improving the system performance in case of time-varying channels (e.g., FSO channels). These hybrid 2*L*-MPPM–*M*DPSK schemes have flexibility to adapt their sensitivity–spectral efficiency tradeoff to cope with changes in the channel state and can change their spectral efficiency gradually (by changing w/N) and not in large discrete steps as in the case of ordinary *M*DPSK or ASK–*M*DPSK schemes. For example, to increase spectral efficiency at the cost of power efficiency, w can be set near $N/2$. On the other hand, if spectral efficiency can be sacrificed for power efficiency, a small value of $w < N/2$ is a better choice.

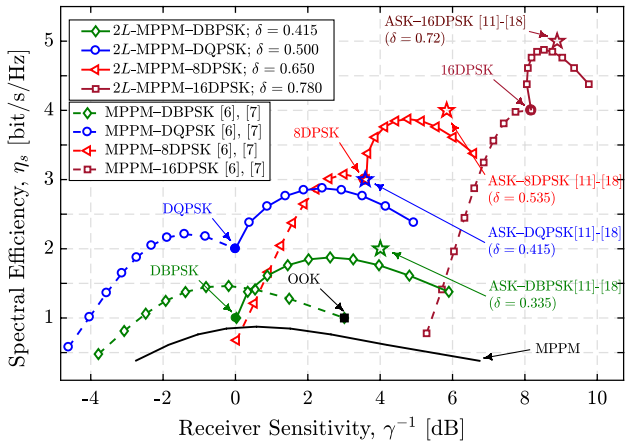

Fig. 3. Achieved spectral efficiencies of different $2L$-MPPM-($N=20$), ASK-, and MDPSK-based modulation techniques versus the receiver sensitivity for different w/N and M.

4. PERFORMANCE UNDER FSO FADING CHANNELS

A. EW-Turbulence FSO Channel Model

Several statistical distributions have been developed to characterize atmospheric turbulence in literature. The most widely accepted distributions are log-normal (LN), gamma-gamma (GG), and EW models [33]. The EW model has been shown to provide excellent matching between simulation and experimental data under a wide range of aperture averaging conditions and turbulence conditions. Moreover, the EW distribution has the attractive feature of simple probability-density function (PDF) and cumulative distribution function (CDF), namely [33],

$$f_h(h) = \frac{\alpha\beta}{\eta}(h/\eta)^{\beta-1}\exp\left(-(h/\eta)^{\beta}\right) \times \left[1-\exp\left(-(h/\eta)^{\beta}\right)\right]^{\alpha-1}, \tag{14}$$

$$F_h(h) = \left[1-\exp\left(-(h/\eta)^{\beta}\right)\right]^{\alpha}, \tag{15}$$

where the receiver-aperture-size-based extra shape parameter α, the scintillation-index (SI)-based shape parameter β, and the scale parameter η are expressed as

$$\alpha \approx 3.931(D_R/\rho_o)^{-0.519}, \tag{16}$$

$$\beta \approx \left(\alpha\sigma_I^2\right)^{-6/11}, \tag{17}$$

$$\eta = \frac{1}{\alpha\Gamma(1+\frac{1}{\beta})g(\alpha,\beta)}, \tag{18}$$

respectively; $\rho_o = (1.46C_n^2(2\pi/\lambda)^2L)^{-3/5}$ is the atmospheric coherence radius, λ is the transmission wavelength, L is the FSO link length, C_n^2 is the refractive-index structure constant, D_R is the aperture diameter, $\Gamma(\cdot)$ is the gamma function, and $g(\alpha,\beta)$ is defined as

$$g(\alpha,\beta) = \sum_{i=0}^{\infty}\frac{(-1)^i(i+1)^{-(1+\beta)/\beta}\Gamma(\alpha)}{i!\Gamma(\alpha-i)}. \tag{19}$$

The parameters of EW PDF are related to the atmospheric parameters through SI as follows:

$$\sigma_I^2 = \frac{\Gamma(1+2/\beta)g_2(\alpha,\beta)}{\alpha(\Gamma(1+1/\beta)g_2(\alpha,\beta))^2} - 1. \tag{20}$$

The value of SI quantifies the strength of fading, i.e., as SI increases, the impact of fading increases.

Using Newton's generalized-binomial theorem and expressing $\exp(\cdot)$ in terms of Meijer G function, $G_{p,q}^{a,b}(\cdot|\cdot)$, via ([34], Eq. (07.34.03.0228.01)), Eq. (14) can be written as

$$f_h(h) = \frac{\alpha\beta}{\eta}\left(\frac{h}{\eta}\right)^{\beta-1}\sum_{j=0}^{\infty}\frac{(-1)^j\Gamma(\alpha)}{j!\Gamma(\alpha-j)}G_{0,1}^{1,0}\left((1+j)\left(\frac{h}{\eta}\right)^{\beta}\Big|_0^-\right). \tag{21}$$

B. Upper-Bound BER Analysis

The $2L$-MPPM symbol consists of w high-signal-level time slots with a power level of P_h and $N-w$ low-signal-level time slots with a power level of $P_l = \delta P_h$, where $0<\delta<1$. The average transmitted optical power P_{av} is defined as

$$P_{\text{av}} = \frac{w+\delta(N-w)}{N}P_h. \tag{22}$$

For ASK, $P_{\text{av}} = 0.5(1+\delta)P_h$.

Upper-bound BER expressions can be derived based on the classical union-bound [35]

$$\text{BER} \le \frac{\kappa}{4}\text{erfc}\left(\frac{d_{\min}}{2\sqrt{N_0}}\right), \tag{23}$$

where $N_0/2$ is the power spectral density of the noise, and κ is the cardinality of the constellation with $\kappa = \binom{N}{w}$, 2, and M for $2L$-MPPM, ASK, and MDPSK techniques, respectively. The minimum Euclidean-distance $d_{\min}$ between any two points in the signal constellation is

$$d_{\min}(h) = \mathcal{R}P_h h \times \begin{cases} \frac{(1-\delta)\sqrt{\tau}}{\sqrt{2}}; & \text{for } 2L-\text{MPPM}, \\ \frac{(1-\delta)\sqrt{\tau}}{2}; & \text{for ASK}, \\ \delta\sin(\pi/M)\sqrt{\tau}; & \text{for } M\text{DPSK}. \end{cases} \tag{24}$$

Accordingly, the upper-bound BER can be written as

$$\text{BER}\,(h) \le \frac{\kappa}{4}\text{erfc}\left(\frac{CP_{\text{av}}}{\sigma_n}h\right), \tag{25}$$

where C is given by

$$C = \begin{cases} \frac{\mathcal{R}(1-\delta)N}{4(w+(N-w)\delta)}; & \text{for } 2L-\text{MPPM}, \\ \frac{\mathcal{R}(1-\delta)}{\sqrt{8}(1+\delta)}; & \text{for ASK}, \\ \frac{\mathcal{R}\delta\sin(\pi/M)N}{\sqrt{8}(w+(N-w)\delta)}; & \text{for } M\text{DPSK}. \end{cases} \tag{26}$$

By expressing $\text{erfc}(\cdot)$ in Eq. (25) in terms of MeijerG function, $G_{p,q}^{a,b}(\cdot|\cdot)$, using {[34], Eq. (07.34.03.0619.01)} and substituting for $d_{\min}(h)$, the BER can be written as

$$\text{BER}\,(h) \le \frac{\kappa}{4\sqrt{\pi}}G_{1,2}^{2,0}\left(\left(\frac{CP_{\text{av}}}{\sigma_n}h\right)^2\Big|_{0,0.5}^{1}\right). \tag{27}$$

The average BER over FSO fading states can be obtained as

$$\mathrm{BER}^{\mathrm{avg}} = \int_0^{\infty} \mathrm{BER}\,(h)\; f_h(h)\mathrm{d}h. \tag{28}$$

By substituting Eqs. (27) and (21) into Eq. (28) and by using {[36], Eq. (21)}, the average BER can be written as Eq. (29):

$$\mathrm{BER}^{\mathrm{avg}} \le \frac{\kappa\alpha\beta\Gamma(\alpha)}{\sqrt{32l}}\left(\frac{P_{\mathrm{av}}}{\sigma_n}\eta C\right)^{-\beta}\sqrt{\frac{kl^{\beta}}{(2\pi)^{l+k-1}}} \times \sum_{j=0}^{\infty}\frac{(-1)^j}{j!\Gamma(\alpha-j)}\mathrm{G}_{2l,k+l}^{k,2l}\left(\left(\frac{1+j}{k}\right)^k\left(\frac{\sqrt{l}\sigma_n}{CP_{\mathrm{av}}\eta}\right)^{2l}\middle|\begin{matrix}\Delta(l,1-\frac{\beta}{2}),\Delta(l,0.5-\frac{\beta}{2})\\ \Delta(k,0),\Delta(l,-\frac{\beta}{2})\end{matrix}\right), \tag{29}$$

where l and k are integers, with $\frac{l}{k}=\frac{\beta}{2}$ and $\Delta(b,a)=\frac{a}{b},\frac{a+1}{b},\cdots,\frac{a+b-1}{b}$.

Finally, an upper-bound on the average BER for the proposed hybrid scheme can be written as

$$\mathrm{BER}^{\mathrm{avg}}_{2L-\mathrm{MPPM}-\mathrm{MDPSK}} \le \frac{\lfloor \log_2\binom{N}{w}\rfloor \mathrm{BER}^{\mathrm{avg}}_{2\mathrm{L}-\mathrm{MPPM}} + N\log_2 M\,\mathrm{BER}^{\mathrm{avg}}_{\mathrm{MDPSK}}}{\lfloor \log_2\binom{N}{w}\rfloor + N\log_2 M},$$

$$\mathrm{BER}^{\mathrm{avg}}_{\mathrm{ASK}-\mathrm{MDPSK}} \le \frac{\mathrm{BER}^{\mathrm{avg}}_{\mathrm{ASK}} + \log_2 M\,\mathrm{BER}^{\mathrm{avg}}_{\mathrm{MDPSK}}}{1+\log_2 M}, \tag{30}$$

where $\mathrm{BER}^{\mathrm{avg}}_{2L-\mathrm{MPPM}}$, $\mathrm{BER}^{\mathrm{avg}}_{-\mathrm{ASK}}$, and $\mathrm{BER}^{\mathrm{avg}}_{M\mathrm{DPSK}}$ can be obtained from Eq. (29) for different values of C given in Eq. (26).

In our analysis, we consider perfect synchronization where the effect of timing error is not considered. However, it is worth noting the expected impact of timing errors on the proposed system performance. There are two types of timing errors: frame-and time-slot-based timing errors. Frame-based timing error is a result of timing offsets that are a multiple of the time-slot duration ($n\tau$; $n\in\{1,2,\cdots,N-1\}$). This type of error has no effect on the performance of the DPSK branch in the proposed scheme, since the relative phase differences between successive slots are not affected by multiple-time-slot offset. The second type of timing error, time-slot timing error, is a result of time offset value $\Delta\tau$, where $\Delta\le 0.5$. The effect of this timing error in DPSK BER performance is discussed and investigated in [37,38], where the effect is considered by multiplying the $\mathrm{BER}^{\mathrm{avg}}_{M\mathrm{DPSK}}$ by factor $\varphi(\Delta)$. In addition, the effect of these two types of timing errors on the MPPM detection process is well known and has been discussed in [39,40].

C. Outage Probability Analysis

The outage probability is defined as

$$\mathrm{P}_{\mathrm{out}} = \Pr(\mathrm{BER}\ge \mathrm{BER}_{\mathrm{th}}) = \Pr(h\le h_{\mathrm{th}}), \tag{31}$$

where h_{th} is the threshold channel gain that guarantees a minimum level of link quality (i.e., $\mathrm{BER}_{\mathrm{th}}$). Rearranging Eq. (25), h_{th} can be bounded as

$$h_{\mathrm{th}} \le \frac{\sigma_n}{CP_{\mathrm{av}}}\mathrm{erfc}^{-1}\left(\frac{4\,\mathrm{BER}_{\mathrm{th}}}{\kappa}\right). \tag{32}$$

Thus, the outage probability can be bounded using Eq. (15) as

$$P_{\mathrm{out}} = \int_0^{h_{\mathrm{th}}} f_h(h)\mathrm{d}h = F_h(h_{\mathrm{th}}) \le \left[1-\exp\left(-\left(\frac{\sigma_n}{C\eta P_{\mathrm{av}}}\mathrm{erfc}^{-1}\left(\frac{4\,\mathrm{BER}_{\mathrm{th}}}{\kappa}\right)\right)^{\beta}\right)\right]^{\alpha}. \tag{33}$$

Finally, the outage probability upper-bound of the FSO systems adopting $2L$-MPPM–MDPSK and ASK–MDPSK schemes is obtained as

$$P^{\mathrm{IM}-M\mathrm{DPSK}}_{\mathrm{out}} \le 1-\left(1-P^{\mathrm{IM}}_{\mathrm{out}}\right)\left(1-P^{M\mathrm{DPSK}}_{\mathrm{out}}\right). \tag{34}$$

5. PERFORMANCE UNDER FIBER NONLINEARITY

A. BER of *M*DPSK Systems Under Fiber Nonlinearity

According to the GN model [29], the impact of fiber nonlinear impairment is modeled as an additive white GN n_{NLI} that is statistically independent of the transmitted signal and the amplified spontaneous emission (ASE) noise [6,29,41–44]. Thus, the total noise at the input of the receiver 3-dB coupler [see Eq. (4) and Fig. 2] is $n_{\mathrm{t}} = n_{\mathrm{NLI}} + n_{\mathrm{ASE}}$, which is a complex zero-mean Gaussian random variable, where n_{NLI} is the noise due to fiber nonlinearity with variance σ^2_{NLI}, and n_{ASE} is the ASE noise with variance σ^2_{ASE}. The variance of n_{t} for the kth time slot can be written as

$$\sigma^2_{tk} = \sigma^2_{\mathrm{ASE}} + \sigma^2_{\mathrm{NLI}k} \tag{35}$$

for

$$\sigma^2_{\mathrm{ASE}} \approx 0.5(G-1)Fh_p\nu B_n N_s, \tag{36}$$

$$\sigma^2_{\mathrm{NLI}k} = \frac{\gamma_f^2}{\pi|\beta_2|}\frac{L^2_{\mathrm{eff}}}{L_{\mathrm{eff,a}}}\frac{B_{\mathrm{n}}N_s}{B^3_{\mathrm{ch}}}P_k^3\,\mathrm{arcsinh}\left(\frac{3\pi^2}{8}L_{\mathrm{eff,a}}|\beta_2|B^2_{\omega}\right), \tag{37}$$

where the average transmitted optical power in the kth time slot is denoted as $P_k\in\{P_l,P_h\}$, which corresponds to $\sigma^2_{tk}\in\{\sigma^2_{tl},\sigma^2_{th}\}$, N_s is number of fiber spans, F is the amplifier noise factor, h_p is Plank's constant, and B_n is the noise bandwidth. The center channel frequency is ν, and G is the amplifier gain that compensates for the span power loss. The total wavelength-division multiplexing (WDM) bandwidth is denoted by $B_\omega = B_{\mathrm{ch}}N_{\mathrm{ch}}$, where B_{ch} is the single-channel bandwidth, and N_{ch} is the number of WDM channels. The fiber nonlinear coefficient is $\gamma_f = 2\pi n_2/(\lambda A_{\mathrm{eff}})$, where n_2 is the nonlinear-index coefficient, λ is the propagating wavelength, A_{eff} is the core effective area, and β_2 is the group-velocity dispersion (GVD). Also, $L_{\mathrm{eff,a}} = 1/2\alpha_f$ and $L_{\mathrm{eff}} = (1-e^{-2\alpha_f L_s})/2\alpha_f$ are the asymptomatic-effective and the effective fiber lengths, respectively, for a single-mode fiber (SMF) attenuation coefficient α_f and a physical fiber span

length L_s. Notice that in this analysis, thermal and shot noises for the fiber case are neglected due to the dominance of the ASE noise over them.

Substituting Eq. (4) into Eq. (6a) and Eq. (6b) and assuming $M=2$ and that the interferometer path difference is equivalent to a time delay of τ, (i.e., $\exp(j\omega_c\tau)=1$), Eq. (7) becomes

$$\begin{aligned} i_k^{\mathrm{DPSK}} &= \mathcal{R}\left(\left|r_{2k}^{\mathrm{DPSK}}\right|^2-\left|r_{3k}^{\mathrm{DPSK}}\right|^2\right)=\frac{\mathcal{R}}{2}\big(a_k a_{k-1}\cos(\Delta\phi_k) \\ &+\mathbb{R}\mathrm{e}\{n_{tk}\}\mathbb{R}\mathrm{e}\{n_{t(k-1)}\}+\mathbb{I}\mathrm{m}\{n_{tk}\}\mathbb{I}\mathrm{m}\{n_{t(k-1)}\} \\ &+a_{k-1}[\mathbb{R}\mathrm{e}\{n_{tk}\}\cos\phi_{k-1}+\mathbb{I}\mathrm{m}\{n_{tk}\}\sin\phi_{k-1}] \\ &+a_k[\mathbb{R}\mathrm{e}\{n_{t(k-1)}\}\cos\phi_k+\mathbb{I}\mathrm{m}\{n_{t(k-1)}\}\sin\phi_k]\big). \end{aligned} \tag{38}$$

Notice that the above analysis for the inphase component can be extended easily in a way similar to the quadrature component for the case of $M>2$ [31]. The first term in Eq. (38), which depends on $\Delta\phi_k$, is the signal to be detected, while the other components, n_d, are treated as noise and distortion terms.

The detected receiver noise variance, σ_d^2, depends on a_k and a_{k-1} and assumes the following cases:

$$\sigma_d^2=\frac{\mathcal{R}^2}{8}\times\begin{cases}\sigma_{tl}^2\sigma_{th}^2+P_h\sigma_{tl}^2+P_l\sigma_{th}^2; & \star,\\ \sigma_{th}^4+2P_h\sigma_{th}^2; & \star\star,\\ \sigma_{tl}^4+2P_l\sigma_{tl}^2; & \star\star\star,\end{cases} \tag{39}$$

where $\star$ denotes the case when $a_k\neq a_{k-1}$, $\star\star$ denotes the case when $a_k=a_{k-1}=A_h$, and $\star\star\star$ denotes the case when $a_k=a_{k-1}=A_l$, as illustrated in Fig. 4. In practice, under constraints on the input power using Eq. (38), the sum of the beating signal-noise term variances (which is a Gaussian random variable) dominates the variance of the noise-noise beating terms, $\mathbb{R}\mathrm{e}\{n_{tk}\}\mathbb{R}\mathrm{e}\{n_{t(k-1)}\}+\mathbb{I}\mathrm{m}\{n_{tk}\}\mathbb{I}\mathrm{m}\{n_{t(k-1)}\}$ (which is a linear combination of Chi-square random variables) [45,46]. In particular, using the parameters in Section 6.B for $P_{\mathrm{av}}\in[-12,4]$ dBm, the signal-noise beating term variance is two orders of magnitude or more larger than the noise-noise beating component. Thus, under these conditions, the total noise, n_d, can be approximated as a Gaussian random variable with variance

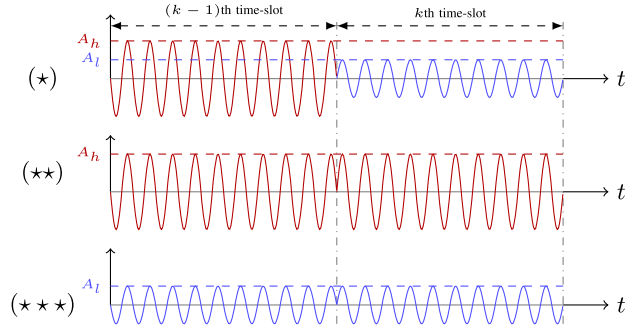

Fig. 4. Time illustration of $\mathbb{R}\{\cdot\}$ part of optical signals for different cases for the amplitude of kth time slot with the amplitude of $(k-1)$th time slot, where $(\star)$ represents $a_k\neq a_{k-1}$, $(\star\star)$ represents $a_k=a_{k-1}=A_h$, and $(\star\star\star)$ represents $a_k=a_{k-1}=A_l$.

$$\sigma_d^2\approx\frac{\mathcal{R}^2}{8}P_h\times\begin{cases}\sigma_{tl}^2+\delta\sigma_{th}^2; & \star,\\ 2\sigma_{th}^2; & \star\star,\\ 2\delta\sigma_{tl}^2; & \star\star\star.\end{cases} \tag{40}$$

In contrast to the FSO channel case, here the noise is dependent of the signal, and a simple worst-case scenario cannot be assumed. For example, in the linear region, case $\star\star\star$ has the lowest signal-to-noise ratio (SNR) given transmission at the lowest DPSK signal power (P_l). Conversely, in the nonlinear region, since the highest DPSK signal power (P_h) is employed, case $\star\star$ has the lowest SNR because the nonlinearity noise variance would be the highest among the three cases.

The average MDPSK BER can be written as

$$\begin{aligned} \mathrm{BER}_{\mathrm{MDPSK}}^{\mathrm{av}} &= \Pr(a_k\neq a_{k-1})\,\mathrm{BER}_{\mathrm{MDPSK}_\star} \\ &+\Pr(a_k=a_{k-1}=P_h)\,\mathrm{BER}_{\mathrm{MDPSK}_{\star\star}} \\ &+\Pr(a_k=a_{k-1}=P_l)\,\mathrm{BER}_{\mathrm{MDPSK}_{\star\star\star}}. \end{aligned} \tag{41}$$

Using Eq. (23), the BER of MDPSK for each of the cases is

$$\mathrm{BER}_{\mathrm{MDPSK}_d}\leq\frac{M}{4}\mathrm{erfc}\left(\frac{\mathcal{R}P_d}{\sqrt{2}\sigma_d}\sin\left(\frac{\pi}{M}\right)\right), \tag{42}$$

where $P_d\in\{\sqrt{P_hP_l}/2,\ P_h/2,\ P_l/2\}$ for cases $\star$, $\star\star$, and $\star\star\star$, respectively, and σ_d^2 is given in Eq. (40).

The likelihood of the cases depends on the IM employed. For $2L$-MPPM,

$$\begin{aligned} &\Pr(a_k\neq a_{k-1})=\Pr(a_k=A_l)\Pr(a_{k-1}=A_h) \\ &+\Pr(a_k=A_h)\Pr(a_{k-1}=A_l)=\frac{2w(N-w)}{N^2}, \qquad (\star) \\ &\Pr(a_k=a_{k-1}=A_h)=\Pr(a_k=A_h)\Pr(a_{k-1}=A_h) \\ &=\frac{w^2}{N^2}, \qquad (\star\star) \\ &\Pr(a_k=a_{k-1}=A_l)=\Pr(a_k=A_l)\Pr(a_{k-1}=A_l) \\ &=\frac{(N-w)^2}{N^2}. \qquad (\star\star\star) \end{aligned}$$

For ASK–MDPSK modulation techniques, the likelihoods for the three cases $\star$, $\star\star$, and $\star\star\star$ are 1/2, 1/4, and 1/4, respectively.

B. BER of 2L-MPPM Systems Under Fiber Nonlinearity

As was done for the MDPSK case in Section 5.A, the signal-noise beating term in Eq. (5) is dominant and modeled as Gaussian distributed with variance

$$\sigma_k^2=\frac{\mathcal{R}^2}{2}a_k^2\sigma_{tk}^2. \tag{43}$$

Using the union bound approximation [35,47], the BERs of $2L$-MPPM and ASK, with different noise variances for different slot power intensities, can be written as

$$\text{BER} \le \begin{cases} \frac{\binom{N}{w}}{4}\text{erfc}\left(\frac{\mathcal{R}P_b(1-\delta)}{2\sqrt{2(\sigma_b^2+\sigma_l^2)}}\right); & \text{for } 2L\text{−MPPM}, \\ \frac{1}{2}\text{erfc}\left(\frac{\mathcal{R}P_b(1-\delta)}{2\sqrt{2}(\sigma_b+\sigma_l)}\right); & \text{for ASK}, \end{cases} \quad (44)$$

where, from Eq. (43), $\sigma_b^2 = \frac{\mathcal{R}^2}{2}P_b\sigma_{tb}^2$ and $\sigma_l^2 = \frac{\mathcal{R}^2}{2}P_l\sigma_{tl}^2$. Finally, the BER of hybrid schemes under fiber nonlinearity can be calculated by substituting Eqs. (41) and (44) in Eq. (29).

6. NUMERICAL RESULTS

A. FSO Channel Results

In this subsection, the BER and outage probability of FSO systems adopting $2L$-MPPM–MDPSK techniques are numerically evaluated using Eqs. (29) and (34), respectively. In addition, the results are verified using Monte Carlo (MC) simulation by directly generating 10^7 fading states and averaging. The operating wavelength of $\lambda = 785$ nm is selected so that silicon PDs can be used in order to decrease the receiver cost. A strongly turbulent FSO channel is considered with $C_n^2 = 2.128 \times 10^{-14}$ m$^{-2/3}$, $L = 1.2$ km, Rytov variance $\sigma_R^2 = 1.3089$, and $\rho_o = 9.4$ mm.

The effect of aperture averaging takes place if $D_R \gg \rho_o$. In order to investigate the effect of aperture averaging on FSO system performance, three different aperture sizes are considered in this section: ($D_R = 3$ mm, $\alpha = 5.44$, $\beta = 0.76$, $\eta = 0.31$, $\sigma_I^2 = 0.4821$), ($D_R = 25$ mm, $\alpha = 4.65$, $\beta = 1.17$, $\eta = 0.52$, $\sigma_I^2 = 0.2126$), and ($D_R = 60$ mm, $\alpha = 3.19$, $\beta = 2.61$, $\eta = 0.82, \sigma_I^2 = 0.0571$) [48].

Figure 5 shows the effect of changing the power ratio δ on outage probabilities. From Eqs. (32) and (26), the outage performance of $2L$-MPPM techniques is improved by decreasing δ, while MDPSK outage is improved by increasing δ. At low δ, MDPSK dominates outage; therefore, by increasing δ, the system performance is improved until an optimum point is reached, balancing the outage of MDPSK and IM techniques. Increasing δ beyond this optimum point results in IM techniques dominating outage, and the total system performance is degraded again.

The outage probability, with $\text{BER}_{\text{th}} = 10^{-3}$, and the average BER versus the average transmitted optical power P_{av} for

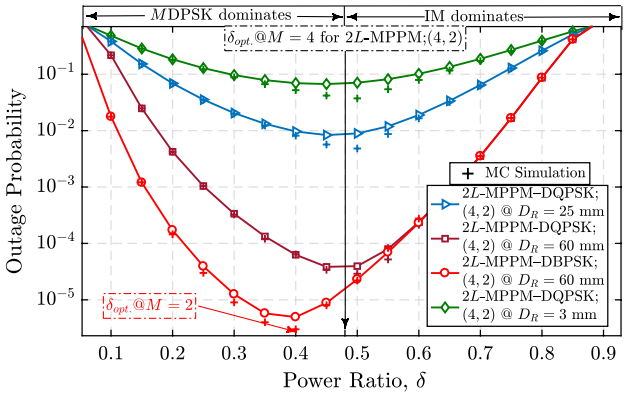

Fig. 5. FSO: outage probabilities versus the power ratio δ for $2L$-MPPM–MDPSK with (N, w) at $P_{\text{av}} = -15$ dBm and $\sigma_n^2 = 25 \times 10^{-14}$ A^2 for different receiver aperture sizes and $\text{BER}_{\text{th}} = 10^{-3}$. MC simulations (+) are also plotted.

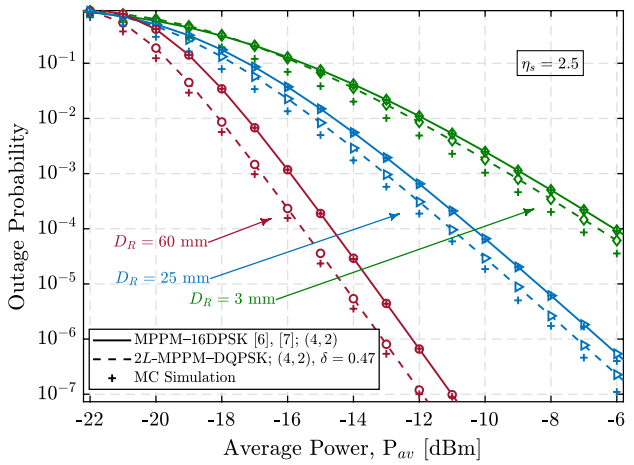

Fig. 6. FSO: outage probability versus average transmitted power P_{av} [dBm] for different FSO channel conditions with different aperture sizes $D_R \in \{3, 25, 60\}$ mm at BER_{th} of 10^{-3} and $\sigma_n^2 = 25 \times 10^{-14}$ A^2 for both $2L$-MPPM–MDPSK with $(N, w, M, \delta, \eta_s) = (4, 2, 4, 0.47, 2.5)$ and MPPM–MDPSK with $(N, w, M, \eta_s) = (4, 2, 16, 2.5)$. MC simulations (+) are also plotted.

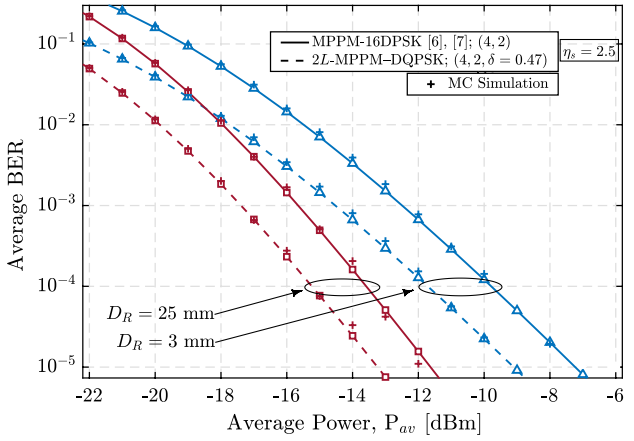

Fig. 7. FSO: Average BER versus average transmitted power P_{av} [dBm] at different aperture sizes $D_R \in \{3, 25\}$ mm for $2L$-MPPM–MDPSK with $(N, w, M, \delta, \eta_s) = (4, 2, 4, 0.47, 2.5)$ and MPPM–MDPSK with $(N, w, M, \eta_s) = (4, 2, 16, 2.5)$. MC simulations (+) are also plotted.

$2L$-MPPM–MDPSK, and traditional MPPM–MDPSK techniques are shown in Figs. 6 and 7 with δ fixed at the optimum value in Fig. 5. To permit a fair comparison, the parameters are chosen so that compared systems have the same spectral efficiency. It can be seen in Figs. 6 and 7 that $2L$-MPPM–MDPSK outperforms intensity–MDPSK by 1 dB at $\eta_s = 2.5$ bit/s/Hz, outage probability$=10^{-3}$ and $D_R = 60$ mm, and by 2 dB at $\eta_s = 2.5$ bit/s/Hz and BER$= 10^{-4}$ for all aperture sizes, respectively. This can be explained since $2L$-MPPM–MDPSK continuously sends DPSK symbols every τ slot interval, while MPPM–MDPSK sends discrete DPSK symbols only in the w non-zero time slots. Therefore, in order to have the same spectral efficiency, MPPM–MDPSK must send higher cardinality DPSK constellations. This increase in MDPSK constellation

size leads to a decrease in the minimum Euclidean distance between MDPSK constellation points. On the other hand, using the nonzero level in the $2L$-MPPM–MDPSK scheme decreases the minimum Euclidean distance between MPPM constellation points. However, by choosing the optimum δ and noting that the majority of hybrid frame bits are encoded using phase modulation, the $2L$-MPPM–MDPSK scheme outperforms MPPM–MDPSK in both BER and outage performance. Additionally, in Figs. 5–7, notice that as D_R increases, aperture averaging is able to mitigate the impact of scintillation. More specifically notice that:

- $2L$-MPPM–MDPSK significantly outperforms MPPM–MDPSK at high spectral efficiencies ($\eta_s \geq 2.25$). However, at lower spectral efficiencies, as shown in Fig. 3, conventional techniques have better power efficiency than the $2L$ approaches.
- Although the case of strong turbulence ($\sigma_R^2 = 1.3089$) is considered here, the outage performance of the proposed system under different levels of turbulence fading can be inferred in Fig. 6. The value of the SI changes depending on the diameter of the receiver aperture via Eq. (20). As the diameter of the receiver aperture increases, the SI decreases due to averaging of the received signal over the aperture. Notice in Fig. 6 that as SI decreases (i.e., increasing aperture) that the gap in performance between $2L$-MPPM–MDPSK and MPPM–MDPSK increases. As the SI reduces, the $2L$-MPPM–MDPSK approaches benefit more due to their smaller Euclidean distance in their MPPM constellations. Overall, however, $2L$-MPPM–MDPSK approaches have stronger performance due to their smaller MDPSK constellations.

B. Optical Fiber Results

The performance $2L$-MPPM–MDPSK on fiber channels is numerically quantified using Eqs. (29), (41), and (44). In addition, the results are verified using MC simulation by generating MPPM symbols and averaging. As with the case for FSO systems, all comparisons are done at the same spectral efficiency by adjusting the parameters for each technique (i.e., N, w, M). The parameters of the fiber system are summarized in Table 3.

Figure 8 plots the variation in the optimum power ratio, δ_{opt}, that balances the performance of $2L$-MPPM and MDPSK to achieve the best BER performance. For each value of average transmitted optical power, P_{av}, δ is swept over the interval (0,1) to find the δ_{opt} that maximizes the SNR and thus minimizes the BER computed via Eqs. (41), (44), and (29). Notice that δ_{opt}

Table 3. Parameter Setting of Optical Fiber Channel [6,45,46]

Parameter	Symbol	Value
Span length	L_s	100 km
Number of spans	N_s	10
Attenuation coefficient	α_f	0.22 dB/km
Dispersion coefficient	D	16.7 ps/km · nm
Nonlinearity coefficient	γ_f	1.3 $\text{W}^{-1}\,\text{km}^{-1}$
Channel bandwidth	B_{ch}	32 GHz
Operating wavelength	λ	1550 nm

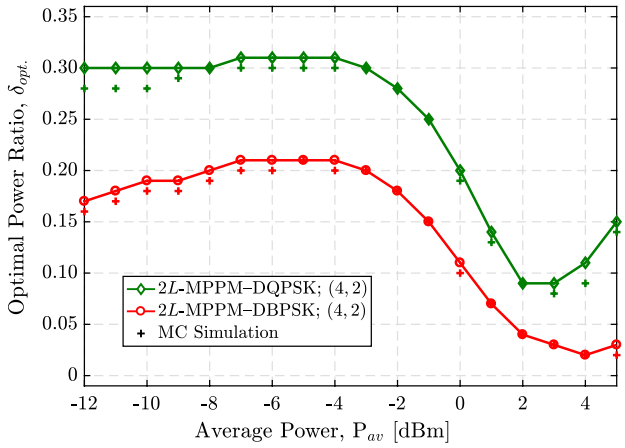

Fig. 8. Fiber: optimal power ratio δ_{opt} versus the average power in (dBm) for (4,2) $2L$-MPPM–MDPSK. MC simulations (+) are also plotted.

varies greatly with P_{av} due to the sensitivity of system performance on both fiber nonlinearity and signal-dependent noise. Qualitatively, at low P_{av} (i.e., in the linear region where only ASE noise exists), δ_{opt} increases with P_{av} to maintain the balance in the performance of MDPSK and MPPM. At larger P_{av}, fiber nonlinearity begins to become significant and system performance is limited by $2L$-MPPM, resulting in a decrease in δ_{opt}. Finally, as P_{av} increases further, the impact of fiber nonlinearity is severe, and δ_{opt} increases again to reduce the high peak power, P_h, to mitigate the effect of nonlinearity.

Figure 9 plots the overall system performance of $2L$ hybrid techniques on a fiber channel. In these simulations, δ is fixed for each modulation scheme corresponding to the δ_{opt} that gives the minimum overall system BER [e.g., Fig. 8 shows an example of (4,2) $2L$-MPPM–DQPSK].

In particular, Fig. 9(a) plots the BER versus the average power P_{av}, while Fig. 9(b) shows the maximum reach versus the average power P_{av} at a BER of 10^{-3}. Notice that the $2L$ approaches provide superior BER and reach over previous hybrid modulation approaches. Specifically, $2L$-MPPM–MDPSK can reach up to 2000 km more than MPPM–MDPSK at $\eta_s = 2.5$ bit/s/Hz and $P_{\text{av}} = -3$ dBm. At high spectral efficiencies, the performance of traditional hybrid techniques is worse than $2L$ techniques due to the need for higher cardinality MDPSK constellations. In addition, at the same average power, the $2L$ techniques have lower peak-to-average-power ratios than traditional MPPM–MDPSK techniques, which relaxes the impact of fiber nonlinearity. Especially, the fiber nonlinearity starts to appear at $P_{\text{av}} = -1$ dBm for the $2L$ techniques, while it starts to appear at $P_{\text{av}} = -3$ dBm for the MPPM–MDPSK technique. Thus, $2L$-MPPM–MDPSK schemes provide a degree of nonlinearity tolerance [specifically, self-phase modulation (SPM), as shown in Fig. 9] compared to MPPM–MDPSK due to their use of smaller constellation size [49,50].

Notice that increasing w for fixed N and fixed P_{av}, in the linear region, would degrade the BER and maximum reach performance, as can be seen in Fig. 3. However, in the nonlinear region, increasing w for fixed P_{av} enhances the performance because the peak power is decreased with increasing w, thus

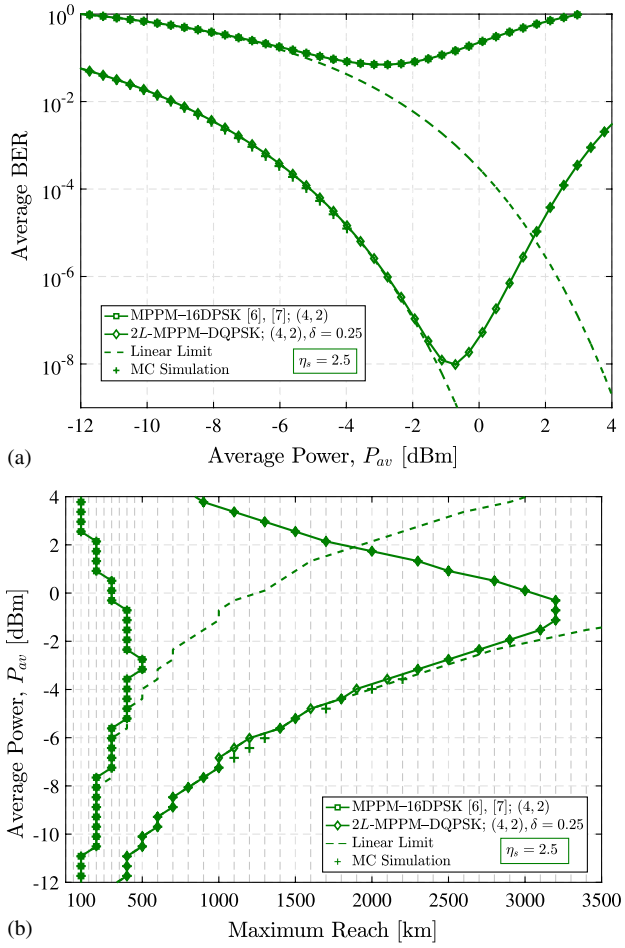

Fig. 9. Fiber: (a) average BER versus average transmitted power P_{av} [dBm] and (b) P_{av} versus maximum achievable reach [km] at a BER of 10^{-3}; for $2L$-MPPM–MDPSK with $(N, w, M, \delta, \eta_s) = (4, 2, 4, 0.25, 2.5)$ and MPPM–MDPSK with $(N, w, M, \eta_s) = (4, 2, 16, 2.5)$. MC simulations (+) are also plotted.

decreasing the effect of fiber nonlinearity. For the FSO channel scenario, the effect of w on the system performance is the same as in the linear region of the fiber channel scenario.

7. CONCLUSION

A simple direct-detection-based hybrid intensity MDPSK modulation technique is proposed in which MDPSK symbols are sent in each slot interval at the cost of some power efficiency in the MPPM sub-modulation. The design and performance of $2L$-MPPM–MDPSK over both FSO and fiber optical channels are investigated. Considering atmospheric scintillation for FSO channels and nonlinearity in fiber channels, we observe significant improvements in system performance at high spectral efficiencies $\eta_s > 2.25$ bit/s/Hz. Over FSO channels, $2L$ modulation techniques provide greater power efficiency at high η_s, e.g., $2L$-MPPM–MDPSK requires approximately 2 dB less power than traditional MPPM–MDPSK for BER$= 10^{-4}$ and $\eta_s = 2.5$ bit/s/Hz. For fiber channels, $2L$ techniques outperform traditional approaches in both BER and transmission reach for high η_s. Specifically, $2L$-MPPM–MDPSK can reach 2000 km farther than MPPM–MDPSK with $P_{\text{av}} = -3$ dBm at $\eta_s = 2.5$ bit/s/Hz and BER$= 10^{-3}$.

Funding. Natural Sciences and Engineering Research Council of Canada; Telus Corporation.

†These authors contributed equally to this work.

REFERENCES

1. X. Liu, S. Chandrasekhar, T. H. Wood, R. W. Tkach, P. J. Winzer, E. C. Burrows, and A. R. Chraplyvy, "M-ary pulse-position modulation and frequency-shift keying with additional polarization/phase modulation for high-sensitivity optical transmission," Opt. Express **19**, B868–B881 (2011).
2. X. Liu, T. H. Wood, R. W. Tkach, and S. Chandrasekhar, "Demonstration of record sensitivities in optically preamplified receivers by combining PDM-QPSK and M–Ary pulse-position modulation," J. Lightwave Technol. **30**, 406–413 (2012).
3. T. A. Eriksson, P. Johannisson, B. J. Puttnam, E. Agrell, P. A. Andrekson, and M. Karlsson, "K-over-L multidimensional position modulation," J. Lightwave Technol. **32**, 2254–2262 (2014).
4. M. Sjodin, T. A. Eriksson, P. A. Andrekson, and M. Karlsson, "Long-haul transmission of PM-2PPM-QPSK at 42.8 Gbit/s," in *OFC/NFOEC Technical Digest*, March 2013, pp. 1–3.
5. H. Selmy, H. M. H. Shalaby, and Z. Kawasaki, "Proposal and performance evaluation of a hybrid BPSK-modified MPPM technique for optical fiber communications systems," J. Lightwave Technol. **31**, 3535–3545 (2013).
6. A. E. El-fiqi, A. E. Morra, S. F. Hegazy, H. M. H. Shalaby, K. Kato, and S. S. A. Obayya, "Performance evaluation of hybrid DPSK-MPPM techniques in long-haul optical transmission," Appl. Opt. **55**, 5614–5622 (2016).
7. A. E. Morra, H. M. H. Shalaby, S. F. Hegazy, and S. S. A. Obayya, "Hybrid direct-detection differential phase shift keying-multipulse pulse position modulation techniques for optical communication systems," Opt. Commun. **357**, 86–94 (2015).
8. H. S. Khallaf, H. M. H. Shalaby, J. M. Garrido-Balsells, and S. Sampei, "Performance analysis of a hybrid QAM-MPPM technique over turbulence-free and gamma-gamma free-space optical channels," J. Opt. Commun. Netw. **9**, 161–171 (2017).
9. H. S. Khallaf, A. E. Elfiqi, H. M. H. Shalaby, S. Sampei, and S. S. A. Obayya, "On the performance evaluation of LQAM-MPPM techniques over exponentiated Weibull fading free-space optical channels," Opt. Commun. **416**, 41–49 (2018).
10. F. Yang, J. Gao, and S. Liu, "Novel visible light communication approach based on hybrid OOK and ACO-OFDM," IEEE Photon. Technol. Lett. **28**, 1585–1588 (2016).
11. E. Tipsuwannakul, P. Johannisson, M. Sköld, E. Agrell, M. Karlsson, and P. A. Andrekson, "Performance comparison of differential 8-ary modulation formats in high-speed optical transmission systems," J. Lightwave Technol. **29**, 2954–2962 (2011).
12. E. Tipsuwannakul, M. Karlsson, E. Agrell, and P. Andrekson, "Performance comparison between 120 Gbit/s RZ-DQP-ASK and RZ-D8PSK over a 480 km link," in *Proceedings of the Optical Fiber Communication Conference*, Los Angeles, CA, 2011, paper OMI5.
13. T. Tokle, M. Serbay, J. B. Jensen, Y. Geng, W. Rosenkranz, and P. Jeppesen, "Investigation of multilevel phase and amplitude modulation formats in combination with polarization multiplexing up to 240 Gb/s," IEEE Photon. Technol. Lett. **18**, 2090–2092 (2006).
14. T. Tokle, M. Serbay, Y. Geng, J. B. Jensen, W. Rosenkranz, and P. Jeppesen, "Penalty-free transmission of multilevel 240 Gbit/s RZ-DQPSK-ASK using only 40 Gbit/s equipment," in *Proceedings of the European Conference on Optical Communication*, Gasglow, U.K., 2005, paper Th.4.1.6.

15. K. Sekine, N. Kikuchi, S. Sasaki, S. Hayase, C. Hasegawa, and T. Sugawara, "40 Gbit/s, 16-ary (4 bit/symbol) optical modulation/demodulation scheme," Electron. Lett. **41**, 430–432 (2005).
16. N. Kikuchi, K. Mandai, and S. Sasaki, "Experimental demonstration of incoherent optical multilevel staggered-APSK (amplitude-and phase-shift keying) signaling," in *Proceedings of the Optical Fiber Communication Conference*, San Diego, CA, 2008, paper OMI3.
17. N. Kikuchi and S. Sasaki, "Incoherent 40-Gbit/s 16QAM and 30-Gbit/s staggered 8APSK (amplitude-and phase-shift keying) signaling with digital phase pre-integration technique," in *Digest of the IEEE/LEOS Summer Topical Meetings*, Acapulco, Mexico, 2008, paper WD3.2.
18. L. N. Binh, *Noises in Optical Communications and Photonic Systems*, 1st ed. (CRC Press, 2016).
19. H. M. H. Shalaby, "Maximum achievable constrained power efficiencies of MPPM-LQAM techniques," IEEE Photon. Technol. Lett. **27**, 1265–1268 (2015).
20. H. S. Khallaf, H. M. H. Shalaby, and Z. Kawasaki, "Proposal of a hybrid OFDM-PPM technique for free space optical communications systems," in *IEEE Photonics Conference (IPC)*, Bellevue, WA, USA, September 2013, pp. 287–288.
21. Y. Sun, F. Yang, and J. Gao, "Comparison of hybrid optical modulation schemes for visible light communication," IEEE Photon. J. **9**, 7904213 (2017).
22. X. Guo, Q. Wang, X. Li, L. Zhou, L. Fang, A. Wonfor, J. L. Wei, J. von Lindeiner, R. V. Penty, and I. H. White, "First demonstration of OFDM ECDMA for low cost optical access networks," Opt. Lett. **40**, 2353–2356 (2015).
23. J. Wei, Q. Cheng, D. G. Cunningham, R. V. Penty, and I. H. White, "100-Gb/s hybrid multiband CAP/QAM signal transmission over a single wavelength," J. Lightwave Technol. **33**, 415–423 (2015).
24. G. Xu, "Error performance of deep space optical communication with M–ary pulse position modulation over coronal turbulence channels," Opt. Express **27**, 13344–13356 (2019).
25. G. Xu, "BER and channel capacity of a deep space FSO communication system using L-PPM-MSK-SIM scheme during superior solar conjunction," Opt. Express **27**, 24610–24623 (2019).
26. M. C. Gökçe and Y. Baykal, "Aperture averaging and BER for Gaussian beam in underwater oceanic turbulence," Opt. Commun. **410**, 830–835 (2018).
27. M. C. Gökçe and Y. Baykal, "Aperture averaging in strong oceanic turbulence," Opt. Commun. **410**, 830–835 (2018).
28. A. E. Elfiqi, A. E. Morra, H. S. Khallaf, H. M. H. Shalaby, and S. Hranilovic, "Two-level MPPM–MDPSK modulation for free-space optical channels," in *Proceedings of the IEEE Globecom*, Abu Dhabi, United Arab Emirates, December 9–13, 2018.
29. P. Poggiolini, A. Carena, G. B. V. Curri, and F. Forghieri, "Analytical modeling of nonlinear propagation in uncompensated optical transmission links," IEEE Photon. Technol. Lett. **23**, 742–744 (2011).
30. M. A. Khalighi and M. Uysal, "Survey on free space optical communication: a communication theory perspective," Commun. Surveys Tuts. **16**, 2231–2258 (2014).
31. K.-P. Ho, *Phase-Modulated Optical Communication Systems* (Springer, 2005).
32. S. Benedetto and E. Biglieri, *Principles of Digital Transmission: With Wireless Applications* (Kluwer, 1999).
33. R. Barrios and F. Dios, "Exponentiated Weibull distribution family under aperture averaging for Gaussian beam waves," Opt. Express **20**, 13055–13064 (2012).
34. Wolfram Function Site, 2018, http://functions.wolfram.com/.
35. S. Haykin, *Communication Systems*, 4th ed. (Wiley, 2001).
36. V. S. Adamchik and O. I. Marichev, "The algorithm for calculating integrals of hypergeometric type functions and its realization in reduce system," in *Proceedings of the International Symposium on Symbolic and Algebraic Computation*, Tokyo, Japan, August 1990, pp. 212–224.
37. M. K. Simon, "A simple evaluation of DPSK error probability performance in the presence of bit timing error," IEEE Trans. Commun. **42**, 263–267 (1994).
38. K. Kiasaleh and T. He, "On the performance of DQPSK communication systems impaired by timing error, mixer imbalance, and frequency nonselective slow Rayleigh fading," IEEE Trans. Veh. Technol. **46**, 642–652 (1997).
39. K. Sato, T. Ohtsuki, I. Sasase, and S. Mori, "Performance analysis of (m, 2) MPPM with imperfect slot synchronization," in *Proceedings of IEEE Pacific Rim Conference on Communications Computers and Signal Processing*, Victoria, BC, Canada, 1993, vol. **2**, pp. 765–768.
40. K. Sato, T. Ohtsuki, and I. Sasase, "Coding for multi-pulse PPM with imperfect slot synchronization in optical direct-detection channels," IEICE Trans. Commun. **E78-B**, 916–922 (1995).
41. W. Shieh and X. Chen, "Information spectral efficiency and launch power density limits due to fiber nonlinearity for coherent optical OFDM systems," IEEE Photon. J. **3**, 158–173 (2011).
42. P. Poggiolini, G. Bosco, A. Carena, V. Curri, Y. Jiang, and F. Forghieri, "A detailed analytical derivation of the GN model of non-linear interference in coherent optical transmission systems," arXiv:1209.0394 [physics] (2012).
43. P. Poggiolini, G. Bosco, A. Carena, V. Curri, Y. Jiang, and F. Forghieri, "The GN-model of fiber non-linear propagation and its applications," J. Lightwave Technol. **32**, 694–721 (2014).
44. G. Bosco, P. Poggiolini, A. Carena, V. Curri, and F. Forghieri, "Analytical results on channel capacity in uncompensated optical links with coherent detection," Opt. Express **20**, 19610–19611 (2012).
45. A. E. Morra, K. Ahmed, and S. Hranilovic, "Impact of fiber nonlinearity on 5G backhauling via mixed FSO/fiber network," IEEE Access **5**, 19942–19950 (2017).
46. A. E. Morra and S. Hranilovic, "Mixed mm wave and radio-over-fiber systems with fiber nonlinearity," IEEE Photon. Technol. Lett. **31**, 23–26 (2019).
47. R. M. Gagliardi and S. Karp, *Optical Communications*, 2nd ed. (Wiley, 1995).
48. R. Barrios, "Exponentiated Weibull fading channel model in free-space optical communications under atmospheric turbulence," Ph.D. thesis (Universitat Politecnica de Catalunya, 2013).
49. P. Serena, A. Bononi, and N. Rossi, "The impact of the modulation dependent nonlinear interference missed by the Gaussian noise model," in *The European Conference on Optical Communication (ECOC)*, Cannes, 2014, pp. 1–3.
50. T. Xu, N. A. Shevchenko, D. Lavery, D. Semrau, G. Liga, A. Alvarado, R. I. Killey, and P. Bayvel, "Modulation format dependence of digital nonlinearity compensation performance in optical fibre communication systems," Opt. Express **25**, 3311–3326 (2017).